Brain Uptake of Thallium-201 from the Cerebrospinal Fluid Compartment

Joseph A. Rubertone, David V. Woo, Jacqueline G. Emrich and Luther W. Brady

Department of Radiation Oncology and Nuclear Medicine, Department of Anatomy, Hahnemann University School of Medicine, Philadelphia, Pennsylvania

The present report elucidates the movement of ^{201}Tl through the cerebrospinal fluid compartment and its subsequent uptake by normal brain. Autoradiographic studies of rat brain, after stereotaxic ^{201}Tl injection into either the lateral or fourth ventricle, reveal that ^{201}Tl moves freely through the cerebrospinal and extracellular fluid compartments. Subsequent to lateral ventricular injection, central thalamic and specific hypothalamic nuclei are heavily labeled. Densely labeled mesencephalic nuclei include the periaqueductal grey and oculomotor nuclear complex. Labeling of giant cells within the vestibular complex is suggestive of neuronal uptake. Major fiber tracts are devoid of label confirming that ^{201}Tl uptake does not occur in white matter. Most labeling following fourth ventricle injection occurs within the caudal medulla and cervical spinal grey. Our findings suggest that ^{201}Tl uptake by normal brain from the cerebrospinal fluid occurs as a function of thallium concentration and neuronal activity.

J Nucl Med 1993; 34:99–103

The usefulness of ^{201}Tl as an imaging agent is due, in part, to the remarkable biochemical and biological similarities shared by the thallous (Tl+) and potassium (K+)ions (*1,2,3*). Thallous has been shown to readily substitute for K+ at the Na+-K+ membrane pump ATPase activation site (*4*) and does not leak out of tissue as rapidly as K+ (*5*). It is nontoxic in radiopharmaceutical dosages (*6*); and has a whole-body clearance half-time of 9.8 days (*7*). Its potential use for tumor detection was realized when lung carcinoma was revealed by myocardial thallium scans (*8*). Its usefulness as a tumor imaging agent was subsequently evaluated and confirmed for neoplastic lesions of the lung (*9*), thyroid, liver (*10*) and brain (*11,12*).

Brain tumor uptake is a combined function of blood-brain barrier (BBB) permeability (*11,12*), and cell viability in terms of increased cell growth and concomitant enhancement of Na+-K+ ATPase activity (*13–16*). Human glioma cells have inward rectifying K+ channels that are 2–5 times more permeable to Tl+ than to K+ (*17*). The presence of an intact BBB in surrounding normal tissue accounts for minimal cerebral uptake (*11,12,18*). Unlike CT or MRI contrast enhancement, which are solely dependent on breakdown of the BBB, ^{201}Tl tumor cell uptake allows for an accurate assessment of intracerebral neoplastic events (*18*). It is superior to [^{99m}Tc]pertechnetate (*11, 12*), ^{99m}Tc-glucoheptonate, and ^{67}Ga-citrate (*19*). Advantages are its ability to: image small metastatic lesions (*11, 12*); detect tumors of mixed histology (*18*); delineate central necrosis from viable tissue (*19,20*); and evaluate tumor recurrence (*21*). Recent ^{201}Tl SPECT studies suggest that they can be used to define tumor grade (*18*) and may be superior to histologic methods (*22*).

Although minimal normal cerebral uptake is a consistent finding (*21*), there is evidence that ^{201}Tl does enter the extracellular fluid (ECF) and CSF compartments. The hypothyseal region (*11,12*) and venous sinuses (*19*) are hyperactive following intravenous injection of ^{201}Tl. Free Tl+ may be entering these compartments via circumventricular organs which lack a BBB. Highly vascularized areas such as the subfornical organ, suproptic crest, median eminence, pineal body, neurohypophysis and area postrema (*23*) may all be serving as ^{201}Tl conduits to the CSF.

Hydrated ionic radius defines ionic movement through solution, and K+ and Tl+ have almost identical radii (*4*). Since K+ moves freely from CSF to ECF compartments (*24*), one can speculate that Tl+ will also move into the ECF. Since ^{201}Tl SPECT imaging indices are based on homologous contralateral normal brain (*22*), knowledge of the movement of ^{201}Tl through the CSF and ECF compartments, and subsequent uptake by normal neuropil is essential.

The purposes of this study were to determine:

1. If ^{201}Tl readily enters the ECF from the CSF.
2. If ^{201}Tl uptake could be correlated to activity.
3. If there is evidence for neuronal uptake.
4. If there are areas that show consistent uptake.
5. If there is evidence for uptake by white matter.

MATERIALS AND METHODS

A total of 20 adult male Sprague-Dawley rats (250–300 g) were used in this study. Animals were anesthetized with a Ketamine (98%)-Acepromazine (2%) solution, placed in a Kopf stereotaxic

Received Mar. 10, 1992; revision accepted Aug. 17, 1992.

For reprints or correspondence contact: Joseph A. Rubertone, PhD, Department of Anatomy, Mail Stop #408, Hahnemann University School of Medicine, Broad and Vine, Philadelphia, PA 19102-1192.

instrument, and prepared for injection using aseptic techniques. Fluid balance and normal body temperature were maintained by subcutaneous injections of lactated Ringers (3.0 ml) and use of a heating pad.

Thallium-201 (50 μl, 50–150 μCi) was injected either into the lateral or fourth ventricle at a rate of 5 μl every 5 min to minimize any drastic increases in CSF pressure. Lateral ventricle injections (n = 10) were done stereotaxically with a 22-gauge blunt needle affixed to a 100 μl Hamilton syringe. The needle was allowed to remain in place 1 hr postinjection. The needle was slowly withdrawn (5 mm every 5 min) to minimize suction along the needle tract during extraction. Fourth ventricle injections (n = 10) were done by placing a small guide hole with a 26-gauge needle into the atlantooccipital membrane. A blunt 22-gauge needle was then placed into this hole with the aid of an operating microscope. This needle was stereotaxically lowered to a point 1.5 mm beneath the atlantooccipital membrane, then slowly withdrawn 0.5 mm. This procedure provides for a tight junction between the needle and the membrane and eliminates the possibility of seepage during injection.

Unconscious animals were exsanguinated 1 to 5 hr postinjection (n = 4 for each hour) via trans-aortic cannulation with a buffered (pH 7.3) saline solution, and immediately perfused with a 4.0% formaldehyde 0.1 *M* phosphate buffer solution (pH 7.4). Brains and spinal cords were cut in 40 μm transverse frozen sections, taken every 250 μm and mounted on acid-cleaned, gel-subbed slides. Mounted sections were allowed to air dry overnight or were placed on a slide warmer for several hours. Dry slides were apposed to LKB Ultrofilm (Broman, Sweden) in standard x-ray cassettes. Radioactive standards (5 mm diameter filter paper discs) were spotted with a known dpm of radioactivity, placed on slides, and developed with the tissue sections for visual comparison with labeled areas. Exposure times ranged from 5 to 7 days. Ultrofilm was developed in Kodak D-19 developer and standard fixation procedures were followed. Tissue sections were stained with Neutral Red for direct histological comparison with corresponding autoradiograms (ARGs).

RESULTS

Regardless of postinjection time intervals, movement of ^{201}Tl occurred throughout the ventricular system subsequent to lateral ventricle injection. The tracer passed through the interventricular foramen of Monroe, the third ventricle (3, Fig. 1A,B), the cerebral aqueduct (ca.) (Fig. 1C,D) and the rostral one-half of the fourth ventricle (4, Fig. 2). The caudal one-half of the fourth ventricle and the cervical spinal cord are only labeled by ^{201}Tl following fourth ventricle injection (Fig. 3).

Subsequent to ^{201}Tl lateral ventricle injection, the cerebral cortex (CC) is virtually devoid of Tl+, while the hippocampal formation (HF) shows marked uptake (Fig. 1B). Certain nuclear groups within the diencephalon are more heavily labeled than others (Fig. 1B). The lateral dorsal (ld), the medial habenular (mhb), paraventricular (pv), centromedial (cm), rhomboid (rh) and reuniens (re) thalamic nuclei are densely labeled. In contrast, the ventroposterolateral (vpl) nucleus shows negligible uptake. The arcuate (arc), dorsal (dh) and ventromedial (vmh) hypothalamic nuclei are consistently labeled, as are the

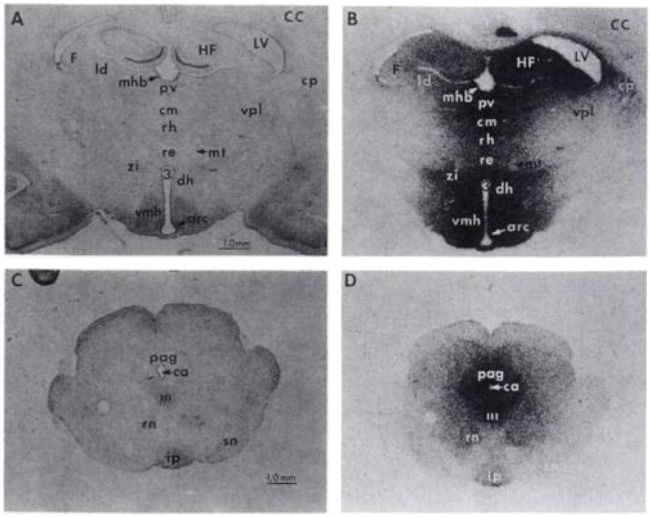

FIGURE 1. Transverse, neutral red stained sections and corresponding autoradiographs at levels of the caudal diencephalon (A,B) and mesencephalon (C,D) representing distribution of ^{201}Tl following lateral ventricle injection. Abbreviations for specific brainstem nuclei are: arc = arcuate, cm = centromedian, cp = caudoputamen, dh = dorsal hypothalamic, ip = interpeduncular, ld = lateral dorsal, mhb = medial habenular, III = oculomotor complex, pv = paraventricular, re = reuniens, rn = red nucleus, rh = rhomboid, and vpl = ventroposterolateral. Other structures indicated are: CC = cerebral cortex, ca = cerebral aqueduct, F = fornix, LV = lateral ventricle, HF = hippocampal formation, mt = mammillothalamic tract, pag = periaqueductal gray, sn = substantia nigra, zi = zona incerta and 3 = third ventricle. All scale lines = 1.0 mm.

zona incerta (zi) and caudoputamen (cp). The mammillothalamic tract (mt) is conspicuous in its absence of ^{201}Tl.

Topographically distinguishable nuclear groups with an affinity for ^{201}Tl are also found in the mesencephalon, cerebellum, pons and rostral medulla following lateral ventricle injection. Densely labeled nuclei in the mesencephalon (Fig. 1D) include the periaqueductal gray (pag) and the oculomotor nuclear complex (III). The interpeduncular nucleus (ip), red nuclei (rn), and substantia nigra (sn) show more modest uptake. Regions of marked ^{201}Tl uptake in the cerebellum are the cerebellar vermis (CV, Fig. 2B), the dorsal lateral hump (dlh) of the ni (Fig. 2D) and the medial (nm), interposed (ni), and lateral (nl) cerebellar nuclei (Fig. 2A–D). The dorsal cochlear nuclei (dc) and the lateral (lv), medial (mv), and spinal (spv) vestibular nuclei are the most densely labeled structures in the pons and rostral medulla. The resolution obtained by the methodology applied allowed for imaging of the giant neurons (Fig. 2A and 2B, arrow heads) characteristically found in the lv (*25*). The restiform body (rb) and spinal trigeminal tract (stV) are clearly delineated by their lack of ^{201}Tl absorption (Fig. 2B, 2D). Myelinated fiber bundles such as the genu (g7) and root of the facial nerve (r7) did not exhibit uptake (Fig. 2B).

Thallium-201 uptake and distribution following fourth ventricle injection are shown in Figures 3B and 3D. Most

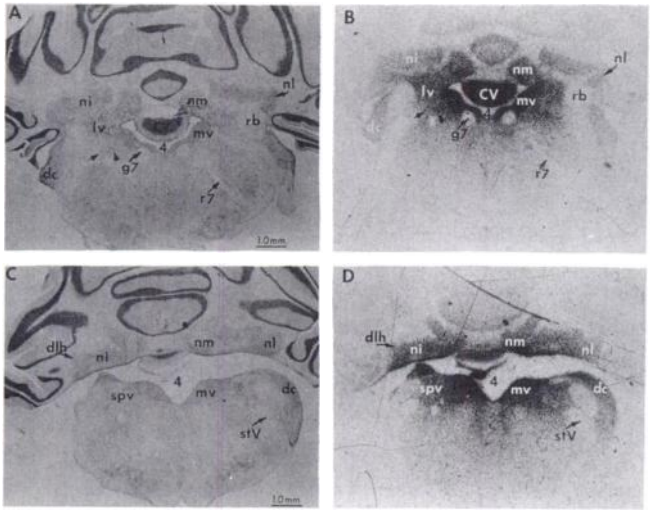

FIGURE 2. Transverse, neutral red stained sections and corresponding autoradiographs at levels of the caudal pons and cerebellum (A,B) and rostral medulla and cerebellum (C,D) representing distribution of ^{201}Tl following lateral ventricle injection. Abbreviations for brainstem and cerebellar nuclei are: dc = dorsal cochlear, dlh = dorsal lateral hump, lv = lateral vestibular, mv = medial vestibular, ni = nucleus interpositus, nl = nucleus lateralis, nm = nucleus medialis, and spv = spinal vestibular. Other indicated structures are: CV = cerebellar vermis, rb = restiform body, stV = spinal tract of the trigeminal nerve, g7 and r7 = genu and root of the facial nerve, and 4 = fourth ventricle. All scale lines = 1.0 mm.

labeling occurs within the caudal medulla and cervical spinal cord. There is no evidence of uptake rostral to the caudal one-half of the fourth ventricle. In the case shown (Fig. 3), the injection was made to the left of the midline.

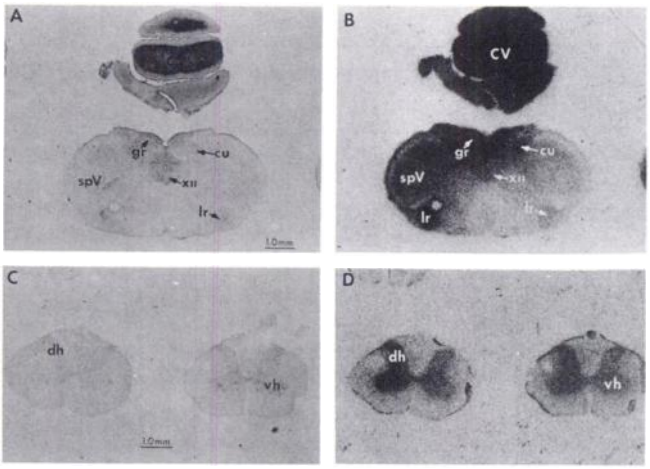

FIGURE 3. Transverse, neutral red stained sections and corresponding autoradiographs (ARGS) at levels of the caudal medulla (A,B) and spinal cord (C,D) representing distribution of ^{201}Tl following fourth ventricle injection. Abbreviations for specific brainstem nuclei are: cu = cuneate, gr = gracile, lr = lateral reticular, spV = spinal nucleus of the trigeminal nerve, and XII = hypoglossal nuclei. Structures labeled in the spinal gray matter are: dh = dorsal horn and vh = ventral horn. All scale lines = 1.0 mm.

In the caudal medulla, the spinal trigeminal (spV), gracile (gr), cuneate (cu), hypoglossal (XII), and lateral reticular nuclei (lr) are well defined. Increased labeling density on the left side of the medulla is due to the proximity of the ^{201}Tl injection. Correlation of tracer proximity and concentration of labeling is emphasized by uptake within the lateral reticular nuclei (lr) (Fig. 3B). The left lr is densely labeled, while the right shows moderate uptake. The cervical spinal gray is clearly defined with dense labeling in the dorsal (dh) and ventral horns (vh). This labeling pattern existed to the level of the fourth cervical segment (Fig. 3D), where spinal grey matter is easily demarcated from adjacent fasciculi. The cerebellar vermis (CV, Fig. 3B) is densely labeled following fourth ventricle injection.

DISCUSSION

Our data show that once ^{201}Tl enters the CSF compartment, it is distributed in accordance with CSF flow dynamics (*23*). After injected into the lateral ventricle, ^{201}Tl is swept downstream through the foramina of Monroe to the third ventricle, and then to the rostral half of the fourth ventricle via the cerebral aqueduct. Injection pressure did not disrupt normal CSF flow, since there is no appreciable upstream labeling following fourth ventricle injection. Labeling of various basal ganglia, brainstem and cerebellar nuclei illustrates the ease with which ^{201}Tl enters the ECF compartment. This observation corroborates the assumption that there is no significant barrier at the pial or ependymal surface (*26–28*).

The movement of ions through solutions and cell membranes is a function of their hydrated and crystalline ionic radii, (*3,4*). Since the hydrated and crystalline radii of K+ and Tl+ are almost identical, there is a great similarity in their ionic movements (*2*). However, important differences do exist between Tl+ and K+ concerning Na+-K+ ATPase pump activation site affinity and influx/efflux activity. Thallous ion is more membrane permeable (*17*) because it has a tenfold greater affinity for the Na+-K+ activation site than K+ (*4*). Although K+ easily passes in and out of cells with change in membrane potential (*24, 29*), Tl+ remains within the cell longer after influx occurs (*5*). This may be due to its greater affinity for nuclear, mitochondrial, and microsomal sites (*2,30*). Our experimental paradigm substantiates that intracellular binding of Tl+ does occur. Since Tl+ is flushed out of the ECF during perfusion, the image observed in our ARGs is due to intracellularly bound ^{201}Tl.

Left fourth ventricle injections result in a preponderance of ipsilateral label supporting the postulate that inward ionic flow is dependent on ECF ionic concentration (*17, 31*). However, concentration gradient is not the only variable dictating Tl+ uptake (*16*).

Since Tl+ behaves like K+ during electrical stimulation (*3*), its uptake may be attributed to neuronal activity. Following right ventricular injection of ^{201}Tl, the right HF is densely labeled, as are the midline thalamic and hy-

pothalamic nuclei. The vpl, although surrounded on three sides by heavily labeled nuclei, has almost no label. Since the vpl is located right next to the injection site and is cytoarchitecturally similar to adjacent labeled nuclei (*23*), the lack of label in the vpl cannot be explained by concentration gradient or neuronal composition. The midline thalamic and hypothalamic nuclei are associated with autonomic function and are active during the anesthetized state, while the vpl relay sensory impulses to the conscious level and accordingly are inactivated (*23*). The difference in labeling patterns between autonomic and somesthetic nuclei suggests that Tl+ uptake is related to nuclear activity. Carbon-14-deoxyglucose metabolic studies done in both unconscious and conscious animals corroborate this hypothesis. The ^{14}C deoxyglucose ARGs in anesthetized animals are identical to those of the present report. Heavily labeled autonomic nuclei are adjacent to a lightly labeled vpl (*32*). The vpl, on the other hand, is heavily labeled in the awake group (*33*).

Histological comparisons with ARGs suggest active Tl+ uptake by neuronal cell bodies. During neuronal activity there is an influx of Na+ and an efflux of K+ (*23*). The excess Na+ serves as a stimulus for Na+-K+ ATPase activation, suggesting that most of the released K+ is pumped right back into the neuron after discharge (*28*). The assumption that neurons selectively absorb and retain Tl+ after discharge is supported by thallium's greater membrane permeability (*17*), higher affinity for Na+-K+ ATPase activation sites (*4*), and protein binding properties (*30*). Imaging neurons is a consequence of ion transport, size and composition of adjacent tissue. The giant cells are typically surrounded by fiber bundles and astroglial processes (*25*). Although determination of glial uptake is beyond the resolution of this study, the possibility that uptake occurs is highly likely. Glia undergo slow depolarizing potentials during times of neuronal activity (*28*), and are responsible for K+ regulation in the ECF compartment (*24*), by intracellularly transporting K+ from areas of high to low concentration (*26*). The distinction between grey and white matter was clear at all brainstem levels studied. Similar results are obtained when Tl+ is conjugated to highly lipophilic compounds (*34*), which allow Tl+ to cross the BBB. The lack of uptake by white matter is explained by the location of influx sites. These sites are located on the entire surface of dendrites, cell bodies, and unmyelinated fibers. Myelinated fibers only show ionic activity at the nodes of Ranvier, with little, if any, K+ influx through the myelin itself (*23*) explaining the consequent lack of ^{201}Tl uptake in white matter observed in the present study.

These data have important clinical implications. Once ^{201}Tl enters the CSF compartment, it gains easy access to the ECF compartment and is readily taken up by normal brain. This uptake may be a function of neuronal activity. The consistent finding of "hyperactive" normal brain areas in clinical imaging studies indicates that normal brain uptake does occur as early as five minutes after intravenous injection (*11,12,19*). Little or no uptake by normal brain surrounding cerebral tumors is usually attributed to the presence of an intact BBB (*11,12*) and to the greater affinity of tumor cells for ^{201}Tl (*17*). Our studies, and others (*35*), reveal that cortex typically has a low affinity for Tl+, and that white matter exhibits little or no Tl+ uptake. Hence, low ^{201}Tl affinity of surrounding normal tissue is a major factor contributing to high cerebral tumor to background ratios. Tumors located in brain areas of high Tl+ affinity would not show nearly as great tumor to normal brain ratios. Evaluation of ^{201}Tl indices (*22*) must address normal brain areas with high ^{201}Tl affinity.

Our data suggest that cellular uptake is influenced by ^{201}Tl ECF concentration. This concentration is directly dependent on capillary flow (*31*). Tumor capillaries often exhibit intermittent flow characteristics, with transient episodes lasting for periods up to 20 minutes (*36*). Thallium-201 ECF concentration in affected areas would presumably be low to nonexistent. Imaging studies performed within 5 min after ^{201}Tl administration (*11,12,18,22,37*) may not allow for an accurate differentiation between chronic and acutely hypoxic areas. This study, and others (*21,38,39,40*), show that Tl+ remains bound within cells for at least one hour after injection. Imaging after this time would allow for visualization of uptake in areas of intermittent flow. Hence, more time between injection and image acquisition would give a more valid indication of tumor viability.

SUMMARY AND CONCLUSIONS

Our data indicate:

1. Once ^{201}Tl gains access to the CSF compartment, it distributes according to CSF flow dynamics, and easily enters the ECF compartment.
2. Thallium-201 uptake appears to be related to neuronal activity.
3. A comparison of ARGs with stained sections suggests that neuronal uptake does occur.
4. There is little or no Tl+ uptake by white matter.
5. Specific neuronal groups show consistent uptake following lateral or fourth ventricle injection.

Our report indicates that the CSF can serve as a potent vehicle for distributing ^{201}Tl throughout the CSF and adjacent ECF compartments. Preliminary studies in our laboratory reveal intense tumor uptake of ^{201}Tl from the CSF compartment (*41*) suggesting a possible regimen for imaging tumors adjacent to, or disseminated within, the ventricular compartment.

ACKNOWLEDGMENTS

The authors would like to express their sincere thanks to Judith Murphy, MD, Director of Nuclear Cardiology, Hahnemann University Hospital, for her advice and procurement of ^{201}Tl, and to

Mr. Arturo Rodriguez and Mr. Joseph Russell for their assistance in handling the isotope. The authors are also indebted to Mr. Edward Yeager for his invaluable help with the photographic segment of the study.

REFERENCES

1. Kawana M, Krizek H, Porter J, Lathrop KA, Charleston D, Harper PV. Use of ^{199}Tl as a potassium analog in scanning [Abstract]. *J Nucl Med* 1970;11:333.
2. Gehring PJ, Hammond PB. The interrelationship between thallium and potassium in animals. *J Pharmacol Exp Ther* 1967;155:187–201.
3. Mullin LJ, Moore RD. The movement of thallium ions in muscle. *J Gen Physiol* 1960;43:759–773.
4. Britten JS, Blank M. Thallium activation of the (Na+-K+)-activated ATPase of rabbit kidney. *Biochim Biophys Acta* 1968;159:160–166.
5. Lebowitz E, Greene MW, Fairchild R, et al. Thallium-201 for medical use. I. *J Nucl Med* 1974;16:151–155.
6. Bradley-Moore PR, Lebowitz E, Greene MW, Atkins HL, Ansari AN. Thallium 201 for medical use. II: biologic behavior. *J Nucl Med* 1975;16: 156–160.
7. Atkins HL, Budinger TF, Lebowitz E, et al. Thallium-201 for medical use. III: human distribution and physical imaging properties. *J Nucl Med* 1977; 18:133–140.
8. Cox PH, Belfer AJ, van der Pompe WB. Thallium-201 chloride uptake in tumors, a possible complication in heart scintigraphy. *Br J Radiol* 1976; 49:767–768.
9. Salvatore M, Carratu L, Porta E. Thallium-201 as a positive indicator for lung neoplasms: preliminary experiments. *Radiology* 1976;121:487–488.
10. Hisada K, Tonami N, Miyamae T, et al. Clinical evaluation of tumor imaging with ^{201}Tl chloride. *Radiology* 1978;129:497–500.
11. Ancri D, Basset JY, Lonchampt MF, Etavard C. Diagnosis of cerebral lesions by thallium-201. *Radiology* 1978;128:417–422.
12. Ancri D, Basset J. Diagnosis of cerebral metastases by thallium-201. *British J Radiol* 1980;53:443–453.
13. Elligsen JD, Thompson JE, Frey HE, Kruuv J. Correlation of (Na+-K+)-ATPase activity with growth of normal and transformed cells. *Exp Cell Res* 1974;87:233–240.
14. Jensen J, Norby JG. Thallium binding to native and radiation-inactivated Na+/K+ ATPase. *Biochim Biophys Acta* 1989;985:248–254.
15. Kasarov LB, Friedman H. Enhanced Na+-K+-activated adenosine triphosphatase activity in transformed fibroblasts. *Cancer Res* 1974;34: 1862–1865.
16. Sehweil AM, McKillop J, Milroy R, Wilson R, Abdel-Dayem HM, Omar YT. Mechanism of ^{201}Tl uptake in tumors. *Eur J Nucl Med* 1989;15: 376–379.
17. Brismar T, Collins VP. Inward rectifying potassium channels in human malignant glioma cells. *Brain Res* 1989;480:249–258.
18. Black KL, Hawkins RA, Kim KT, Becker DP, Lerner C, Marciano D. Use of thallium-201 SPECT to quantitate malignancy grade of gliomas. *J Neurosurg* 1989;71:342–346.
19. Kaplan WD, Takvorian T, Morris JH, Rumbaugh CL, Connolly BT, Atkins HL. Thallium-201 brain tumor imaging: a comparative study with pathologic correlation. *J Nucl Med* 1987;28:47–52.
20. Stafford-Schuck K, Mountz J, McKeever P, Taren J. Thallium-201 localization for residual high grade astrocytoma [Abstract]. *J Nucl Med Technol* 1986;14:Ab9.
21. Mountz JM, Raymond PA, McKeever PE, et al. Specific localization of thallium-201 in human high-grade astrocytoma by microautoradiography. *Cancer Res* 1989;49:4053–4056.
22. Kim KT, Black KL, Marciano D, et al. Thallium-201 SPECT imaging of brain tumors: methods and results. *J Nucl Med* 1990;31:965–969.
23. Carpenter MB, Sutin J. Meninges and cerebrospinal fluid. In: Carpenter MB, Sutin J, eds. *Human neuroanatomy*, 8th edition. Baltimore: Williams & Wilkins; 1983:1–25.
24. Gardner-Medwin AR. A study of the mechanisms by which potassium moves through brain tissue in the rat. *J Physiol* 1983;335:353–374.
25. Mehler WR, Rubertone JA. Anatomy of the vestibular nuclear complex. In: Paxinos G, ed. *The rat nervous system, volume II. Hindbrain and spinal cord.* Orlando: Academic Press; 1985:185–220.
26. Gardner-Medwin AR. Analysis of potassium dynamics in mammalian brain tissue. *J Physiol* 1983;335:393–426.
27. Levin VA, Fenstermacher JD, Patlak CS. Sucrose and inulin space measurements of cerebral cortex in four mammalian species. *Am J Physiol* 1970;219:1528–1533.
28. Varon SS, Somjen GG. Neuron-glia interactions. *Neurosci Res Prog Bull* 1979;17:1–239.
29. Brismar T, Collins VP, Kesselberg M. Thallium-201 uptake relates to membrane potential and potassium permeability in human glioma cells. *Brain Res* 1989;500:30–36.
30. Ando A, Ando I, Katayama M, et al. Biodistribution of ^{201}Tl in tumor bearing animals and inflammatory lesion induced animals. *Eur J Nucl Med* 1987;12:567–572.
31. Charkes DN. Relationship between thallium uptake and blood flow. *J Nucl Med* 1987;28:399–400.
32. Hand PJ. The 2-deoxyglucose method. In: Heimer L, Robards MJ, eds. *Neuroanatomical tract-tracing methods.* New York: Plenum Press; 1981: 511–538.
33. Sokoloff L, Kennedy C, Smith CB. The [14-C] deoxyglucose method for measurement of local cerebral glucose utilization. In: Boulton AA, Baker GB, eds. *Neuromethods, volume 11: Carbohydrates and energy metabolism.* Clifton: Humana Press, Inc; 1989:155–193.
34. de Bruine JF, van Royen EA, Vyth A, de Jong JMBV, van der Schoot JB. Thallium-201 diethyldithiocarbamate: an alternative to iodine-123 N-isopropyl-p-iodoamphetamine. *J Nucl Med* 1985;26:925–930.
35. Rios C, Galvan-Arzate S, Tapia R. Brain regional thallium distribution in rats acutely intoxicated with Tl_2SO_4. *Arch Toxicol* 1989;63:34–37.
36. Chaplin DJ, Durand RE, Olive PL. Acute hypoxia in tumors: implications for modifiers of radiation effects. *Int J Radiat Oncol Biol Phys* 1986;12: 1279–1282.
37. Mountz JM, Stafford-Schuck K, McKeever PE, Taren J, Beierwaltes WH. Thallium-201 tumor/cardiac ratio estimation of residual astrocytoma. *J Neurosurg* 1988;68:705–709.
38. Ochi H, Sawa H, Fukuda T. Thallium-201-chloride thyroid scintigraphy to evaluate benign and/or malignant nodules: usefulness of the delayed scan. *Cancer* 1982;50:236–240.
39. Rubertone JA, Woo DV. Brain imaging studies using thallium 201. *Anat Rec* 1986;214:112A.
40. Sehweil A, McKillop JH, Ziada G, Al-Sayed M, Abdel-Dayem H, Omar YT. The optimum time for tumor imaging with thallium-201. *Eur J Nucl Med* 1988;13:527–529.
41. Rubertone JA, Woo DV. Brain tumor studies using thallium-201. *Anat Rec* 1987;218:117A.